Geomechanics and Engineering, *Vol. 42, No. 2 (2025) 117-127*
https://doi.org/10.12989/gae.2025.42.2.117

Basalt fiber-reinforced controlled low strength material

Dong Geon Son[1] and Yong-Hoon Byun*[2]

[1]*School of Civil, Environmental and Architectural Engineering, Korea University, 145, Anam-ro, Seongbuk-gu, Seoul 02841, South Korea*
[2]*Department of Agricultural Civil Engineering, Kyungpook National University, 80 Daehak-ro, Buk-gu, Daegu 41566, South Korea*

(*Received April 4, 2024, Revised June 27, 2025, Accepted July 4, 2025*)

Abstract. Controlled low-strength material (CLSM) has been developed to enhance the stability of underground structures and overcome the drawbacks of traditional backfill materials, such as compacted sandy soils. The objective of this study is to develop CLSM reinforced with basalt fibers (BF) and to evaluate the flowability, setting time, and strength characteristics of BF-reinforced CLSM. Basalt fibers are incorporated into CLSM with four fiber lengths and three fiber contents to form BF-reinforced CLSM specimens. Flow and Vicat needle tests are performed to evaluate the fluidity and setting times of BF-reinforced CLSM. Uniaxial compression tests and splitting tensile tests are conducted on 3 and 28 days after curing. The results reveal that the incorporation of BF into CLSM reduces the fluidity as well as the initial and final setting times. After 3 days of curing, BF-reinforced specimens with fiber lengths of 18 and 24 mm exhibit higher uniaxial compressive strength than unreinforced specimens; however, at 28 days, the reinforcement effect is marginal. The splitting tensile strength of all reinforced specimens, at both 3 and 28 days, exceeds that of the unreinforced specimens. In particular, at 28 days, the splitting tensile strength of all reinforced specimens generally increases with fiber length. Therefore, the use of BF in CLSM can enhance early compressive strength and improve both early-age and long-term tensile strength in underground structures backfilled with CLSM.

Keywords: basalt fibers; CLSM; splitting tensile strength; uniaxial compressive strength

1. Introduction

In urban areas, a vast network of pipes for water supply and sewage systems is installed underground. In general, the installation and replacement of the pipes involve using coarse granular soils as backfill in narrow trenches, which can cause vibration and noise due to the compaction process. Moreover, the deterioration of the buried pipes can lead to internal erosion, resulting in underground cavities and potential collapse. Thus, the selection of appropriate construction materials for filling the cavities or trenches is essential.

Controlled low-strength material (CLSM) is a flowable cementitious backfill material, which are also used for trench backfilling and void filling. Compared to other fill materials, such as compacted soil, CLSM exhibits higher strength and flowability (Han *et al.* 2019, Xiao *et al.* 2021, Zadehmohamad *et al.* 2021, Gomaa *et al.* 2023, Kim *et al.* 2023). A CLSM mixture typically consists of Portland cement, fly ash, fine aggregate, and water. The fluid consistency of CLSM, which eliminates the need for compaction, is particularly suitable for areas with limited access where filling and achieving compaction can be problematic (ACI 229R, 2005). For CLSM, no visible separation should exist, and the diameter of the spread material should be at least 200 mm. Considering future excavation, CLSM with a compressive strength of less than or equal to 0.3 MPa can be excavated manually. For compressive strengths of 0.7–1.4 MPa, mechanical equipment such as backhoes is used. The maximum long-term compressive strength should be less than 2.1 MPa.

Various studies have investigated the rheological and mechanical characteristics of CLSM. Kim *et al*. (2021) explored the relationship among shear wave velocity, strength, and stiffness according to the type of fly ash in CLSM. Their findings suggested that the monitoring of shear waves in CLSM with varying types of fly ash can reliably predict its strength and stiffness. Byun *et al.* (2016) utilized embedded piezoelectric transducers, including piezoelectric disk and bender elements, to monitor the hydration process of fresh CLSM. Shear wave velocity analysis revealed that the water content of CLSM was related to the interconnection of cementitious particles. Han *et al.* (2019) conducted direct shear tests to evaluate the interface friction angle between soils and CLSM and reported changes in the interface friction angle with respect to the curing time of CLSM and the coefficient of uniformity of soil. Expandable foam grout, developed as a flowable and expandable fill material, has been extensively studied with regard to engineering properties, including stiffness, shear strength, compressive strength, and permanent deformation under cyclic loading (Lee *et al.* 2020, Han *et al.* 2021a, b, 2023). Given the high carbon emissions associated with cement in CLSM, attempts have been made to reduce its usage. Do *et al*. (2016) examined

*Corresponding author, Associate Professor
E-mail: yhbyun@knu.ac.kr

ISSN: 2005-307X (Print), 2092-6219 (Online)

the compressive strength of CLSM in which cement was partially replaced by red mud and reported that the red mud proportion was correlated to the strength increment. Alkali-activated CLSMs in which cement is replaced with different by-products or agricultural waste have been investigated (Lee *et al.* 2013, Park *et al.* 2017, Ghanad and Soliman, 2021, Khadka *et al.* 2023). Recently, Heo *et al*. (2024) investigated flowability, setting time, strength, and shear wave velocity of CLSM integrated with lignosulfonate as an eco-friendly stabilizer.

Numerous researchers have developed various fiber-reinforced cementitious materials and investigated their engineering properties (Kalantari *et al.* 2010, Kalantari and Rezazade 2015, Algin and Ozen 2018, Ahmad *et al.* 2019, Bendjillali *et al.* 2020, Dadmand *et al.* 2020, Cakir *et al.* 2021, Ge *et al.* 2023, Fediuk *et al.* 2023, Okuyucu *et al.* 2019, Shelote *et al.* 2021, Safdar *et al.* 2023). Okuyucu *et al*. (2019) investigated the properties of steel fiber-reinforced CLSMs in pavement base layers under vehicle loading and concluded that the addition of steel fiber enhanced its strength, ductility, and strain capacity while simultaneously providing good constructability. In contrast, basalt fibers (BF) are environmentally friendly and nonhazardous materials, and their production process is less energy-intensive and primarily dependent on the globally abundant basalt rock (Deák and Czigány, 2009; Jamshaid and Mishra, 2016). Algin and Ozen (2018) investigated the properties of self-compacting concrete enriched with BF of varying lengths and identified the optimum volume fraction and length of BF using the response surface method. Shelote et al. (2021) designed an alkali-activated reinforced masonry mortar with BF and determined the optimal mix design. Cakir et al. (2021) evaluated the uniaxial compressive strength and splitting tensile strength of polymer mortars mixed with glass and BF according to the curing time and determined the most efficient mix proportion. However, the potential of integrating BF into CLSM is still unexplored.

In this paper, the compressive and tensile strength characteristics of BF-reinforced CLSM are investigated. First, the characteristics of BF and the mix design of CLSM are introduced. Further, BF with varying lengths and fiber proportions in the CLSM mixture are examined. In addition, the fluidity and setting time are assessed using the flow test and Vicat needle test, respectively. Uniaxial compressive strength and splitting tensile strength tests are conducted as a function of the curing time, highlighting the strength characteristics in relation to the length and amount of BF used. Variations in the uniaxial compressive strength and splitting tensile strength, which are affected by the length of the BF, are subsequently discussed. Finally, scanning electron microscopy (SEM) is employed to verify the distribution of the fiber filaments on the surface of the CLSM mixed with BF.

2. Materials

2.1 CLSM components

Table 1 Chemical compositions of basalt fiber, fly ash, and cement

Oxide [%]	Basalt fiber	Fly ash	Cement
SiO_2	47.6	41.8	18.0
Al_2O_3	14.0	29.9	4.4
Fe_2O_3	11.2	3.7	3.6
CaO	6.9	6.8	61.3
MgO	4.5	1.0	3.4
Na_2O	3.6	0.2	0.2
Others	4.0	5.4	6.1

Table 2 Properties of basalt fibers

Density [g/cm^3]		2.66
Tensile strength [MPa]		1500
Aspect ratio	L= 6 mm	300
	L= 12 mm	600
	L= 18 mm	900
	L= 24 mm	1200

Basalt is a natural substance found in volcanic rocks created by the rapid cooling of lava, with a melting temperature between 1500°C and 1700°C. BF is developed from basalt by the Moscow Research Institute of Glass and Plastic. Because fibers exhibit high electrical insulation, environmental friendliness, and cost efficiency, BFs have been investigated in various engineering fields (Deák and Czigány 2009, Morova 2013). In this study, BFs with lengths of 6, 12, 18, and 24 mm are incorporated into CLSM. Fig. 1 shows the photographs of BF, and Table 1 summarizes the chemical composition of BF as analyzed by X-ray fluorescence. BF predominantly comprise SiO_2, Al_2O_3, and Fe_2O_3 (Table 1), with marginal contents of CaO, MgO, and Na_2O. Based on the SiO_2 content, BF was classified as acidic basalt (Deák and Czigány, 2009). Physical properties of BF are summarized in Table 2. The thickness of a single fiber of BF is 0.02 mm, and the aspect ratios of fibers with a length of 6, 12, 18, and 24 mm are 300, 600, 900, and 1200, respectively. The density of BF is 2.66 g/cm^3, and the tensile strength of BF is 1500 MPa.

In this study, the CLSM comprises ordinary Portland cement, fly ash, sand, and water. The chemical compositions of the cement and fly ash are examined (Table 1). Fly ash primarily comprises SiO_2, Al_2O_3, and Fe_2O_3, with 75.4% of the combined content of these oxides. The CaO content of fly ash is 6.8%; thus, according to ASTM C618 (2015), fly ash is classified as Class F fly ash. Fig. 2 shows the particle size distribution curves of fly ash and sand. The mean diameters (D_{50}) for fly ash and sand are determined to be 0.024 and 1.1 mm, respectively (Table 3). The coefficient of uniformity (C_u) and coefficient of curvature (C_c) of the sand are determined to be 4.02 and 0.86, respectively. According to the Unified Soil Classification System, sand is categorized as poorly graded sand, SP. For CLSM specimens, tap water at approximately 15°C is used.

Table 3 Index properties of sand and fly ash used in this study

Type	Particle sizes corresponding to percent finer [mm]				Coefficient of uniformity	Coefficient of curvature
	D_{10}	D_{30}	D_{50}	D_{60}		
Sand	0.35	0.65	1.07	1.40	4.02	0.86
Fly ash	0.0041	0.012	0.024	0.033	8.18	0.0012

* D_{10} = 10% cumulative passing; D_{30} = 30% cumulative passing; D_{50} = 50% cumulative passing; D_{60} = 60% cumulative passing

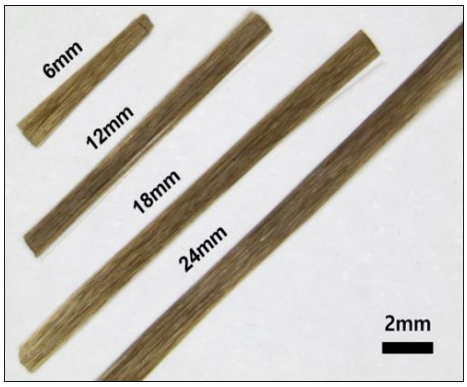

Fig. 1 Photographs of basalt fibers (BF)

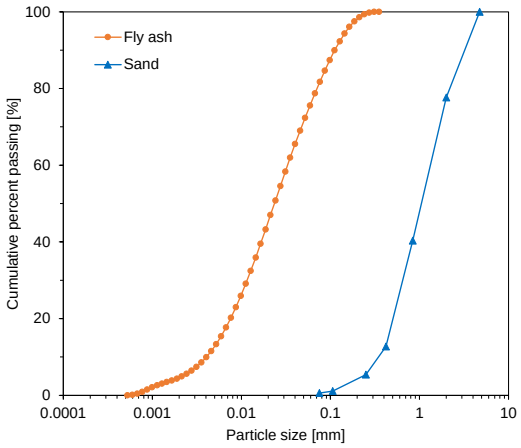

Fig. 2 Grain size distribution curves of sand and fly ash

2.2 Mix design

CLSM is prepared by mixing ordinary Portland cement, fly ash, sand, and water in proportions of 4.8%, 16.4%, 58.6%, and 20.2% of the total weight, respectively. This mix proportion is determined through a trial-and-error process by fixing the fly ash content, reducing the cement content, and adjusting the amount of sand and water. The resulting mixture exhibits no segregation and satisfies the flowability requirements for CLSM. BF with lengths of 6, 12, 18, and 24 mm are added to CLSM at weights of 0.05%, 0.1%, and 0.15% of the total mixtures. With an increase in the BF content, the proportion of sand is adjusted to maintain a 100% mixing ratio. The mixing method involves dry mixing the cement, fly ash, and sand. Next, water is introduced, and the mixture is stirred for approximately 2 min. To ensure the homogeneous dispersion of BF within the CLSM specimens, the mixture is stirred for an additional 2 min.

3. Experimental program

To investigate the flowability, setting time, and compressive and tensile strengths of BF-reinforced CLSM, the flow test, Vicat needle test, uniaxial compression test, and splitting tensile test are conducted. The flow test is performed using a circular mold with a diameter of 75 mm and a height of 150 mm. The flow value of CLSM is determined by averaging the maximum diameter of the spread sample and its corresponding perpendicular diameter, in accordance with ASTM D6103 (1997). The Vicat needle test, based on ASTM C191 (2013), is conducted to evaluate the setting time of CLSM. Over time, the cementitious material underwent hydration, which reduces its fluidity. The time at which a penetration depth of 25 mm is observed is considered as the initial set time, while the time when no trace of the needle is visible is considered as the final set time. To evaluate compressive strength, uniaxial compression tests are conducted using cylindrical specimens with a diameter of 50 mm and a height of 100 mm, following ASTM D4832 (2002). To investigate early- and long-term strengths, the specimens are cured for 3 and 28 days, respectively. To achieve adequate hardening of the specimen, wet curing is applied within the mold. After a 3-day period, the specimen is removed from the mold and subjected to submerged curing at approximately 20°C. A compression testing machine with a loading capacity of 25 kN is used to apply a uniaxial compressive load at a rate of 1 mm/min. To assess the effect of BF on tensile strength, splitting tensile tests are conducted on cylindrical specimens with a diameter of 50 mm and a height of 100 mm, cured for 3 and 28 days. In accordance with ASTM C496 (2004), plywood is placed at both ends of each specimen to ensure uniform load distribution. The test is performed using the same machine as that used for the uniaxial compression test, operating at a rate of 1 mm/min.

4. Results and discussion

4.1 Flowability

A flow test is conducted to evaluate the fluidity of the BF-reinforced CLSM. Fig. 3 shows the variation in flow values as a function of the length and content of BF. The flow value of CLSM without BF is recorded at 346 mm, which is greater than those of all specimens containing BF. Furthermore, the flow value considerably decreases with an increase in the BF content of the specimen, while the

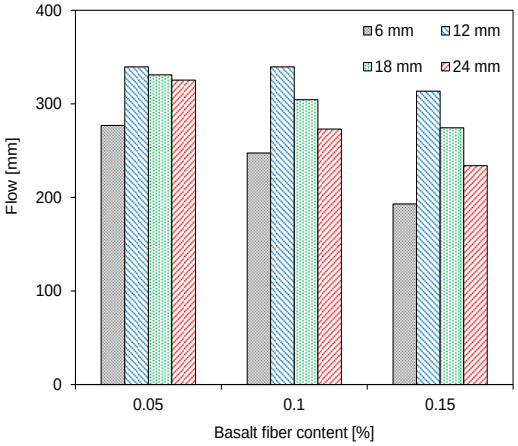

Fig. 3 Variation in the flow of BF-reinforced CLSM with respect to the basalt fiber content

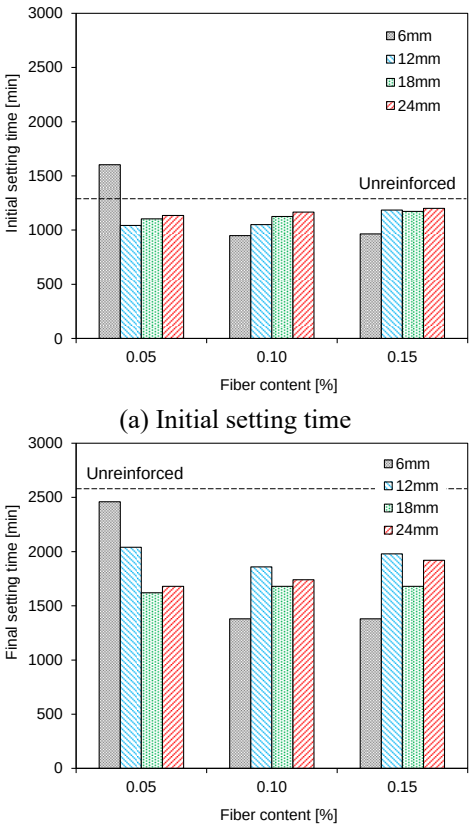

(a) Initial setting time

(b) Final setting time

Fig. 4 Results of Vicat needle tests obtained for BF-reinforced specimens

reduction in the flow value increase with an increase in the BF length, except for CLSM with a fiber length of 6 mm. Previous studies have confirmed that fluidity decreased with the amount of fiber incorporated into cementitious materials (Choi and Yuan 2005, Okuyucu *et al.* 2019, Li *et al.* 2022, Jiang *et al.* 2010, Jiang *et al.* 2014, Afridi *et al.* 2019). Jiang *et al*. (2010) also reported that fluidity decreased when 13-mm-long fibers were mixed into cement mortar, and the fluidity decreased considerably with the fiber content. Similarly, Jiang *et al*. (2014) and Ma *et al*. (2011) conducted slump tests and reported that mixing BF

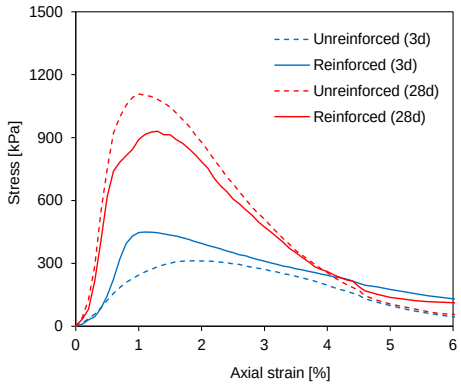

Fig. 5 Stress–strain curves obtained from uniaxial compression tests of unreinforced CLSM and BF-reinformed CLSM after curing for 3 and 28 days with a fiber content of 0.05%

into concrete led to a greater reduction in fluidity, particularly with longer fibers and higher fiber contents. The reduction in fluidity can be attributed to the large specific surface area and rough texture of BF, which increase the internal friction within the cementitious materials. In addition, the incorporated BF absorbs moisture, further contributing to decreased fluidity.

4.2 Setting time

The initial and final setting times are compared to evaluate the setting characteristics of BF-reinforced CLSM (Fig. 4). The black dashed lines represent the initial and final setting times of unreinforced CLSM, respectively. Overall, the initial and final setting times of the BF-containing samples decrease in comparison with those of the samples without fibers. For the same fiber content, with an increase in the fiber length, the initial setting time generally increase, except for CLSM with a fiber content of 0.05% and a fiber length of 6 mm (Fig. 4(a)). Choi and Choi (2021) also found that increasing the content of two different fiber types in cementitious materials resulted in an extended initial setting time for both types of fibers. In this study, with an increase in the fiber content, CLSM with a fiber length of 6 mm exhibits a considerably decreased final setting time (Fig. 4(b)). Xu *et al*. (2021) demonstrated that incorporating BF into a geopolymer grouting material comprising slag and fly ash resulted in a shorter final setting time for the materials blended with shorter basalt fibers. However, for CLSM with fiber lengths of 12, 18, and 24 mm, changes in the final setting time are not considerably affected by different fiber contents. Lee and Lee (2022) demonstrated that for cement mortar mixed with steel fibers, the initial and final setting times decreased with an increase in the steel fiber content. In contrast, Punurai et al. (2018) reported that for geopolymer materials blended with BF, the proportion of BF relative to fly ash led to an increase in the initial and final setting times. Considering that in this study, only a relatively small quantity of BF is incorporated into CLSM compared to that used in previous studies, the added fiber content may be insufficient to render a pronounced effect on the setting times.

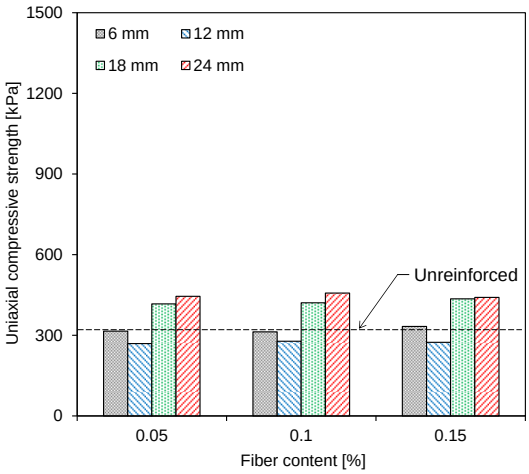

(a) 3 days

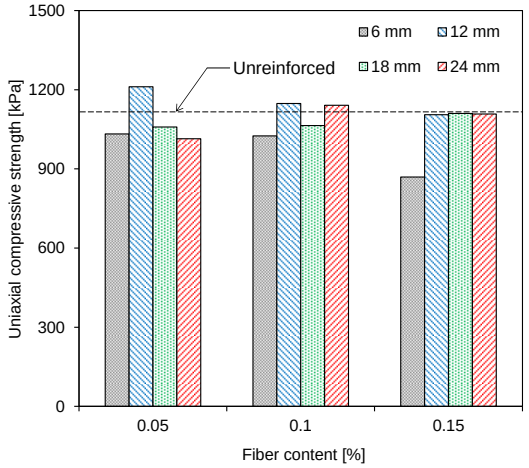

(b) 28 days

Fig. 6 Uniaxial compressive strength at various lengths and contents of basalt fibers

4.3 Uniaxial compressive strength

Fig. 5 shows the typical stress–strain curves of unreinforced CLSM specimens and CLSM specimens reinforced with 24-mm-long BF after 3 and 28 days of curing to investigate their uniaxial compressive strength behaviors. Compared to the unreinforced specimens, BF-reinforced specimens cured for 3 days generally exhibit higher maximum compressive stress, referred to as uniaxial compressive strength. In particular, BF-reinforced CLSM exhibit a considerable increase rate of compressive stress initially, indicative of improved stiffness. The reinforced and unreinforced specimens after 28 days of curing exhibit more rapid increase rates of compressive stress and compressive strength greater than those of specimens after 3 days of curing. For the reinforced specimens after 28 days of curing, the uniaxial compressive strength is less than that of the unreinforced specimens. Choi and Yuan (2005) conducted uniaxial compression tests and reported that the concrete specimens mixed with glass and polypropylene (PP) fibers exhibited reduced compressive strength.

Fig. 6 shows the uniaxial compressive strength of CLSM according to the length and content of BF. The red dashed line represents the uniaxial compressive strength of the specimens without BF, with values of 312 and 1113 kPa at 3 and 28 days after curing, respectively. For 3 days after curing, the BF-reinforced specimens exhibit a rarely noticeable variation in the uniaxial compressive strength as a function of the fiber content, whereas the uniaxial compressive strength is affected by the fiber length (Fig. 6(a)). Compared to the unreinforced specimens, CLSM reinforced with 18- and 24-mm-long fibers exhibit considerably increased uniaxial compressive strengths regardless of the fiber content. The uniaxial compressive strength of the specimens reinforced with 6-mm-long fibers is similar to that of the unreinforced specimens. Fig. 6(b) shows the uniaxial compressive strength of reinforced and unreinforced CLSMs after 28 days of curing, The uniaxial compressive strength apparently increases or decreases depending on the length and content of fibers. With an increase in the fiber content, the uniaxial compressive strength of the specimens reinforced with 6- and 12-mm-long fibers tend to decrease. Lam *et al*. (2015) demonstrated that with an increase in the fiber content of concrete, the strength decreased due to voids created by the flocculation of fibers. In contrast, the uniaxial compressive strength of the specimens reinforced with 18-mm-long fibers increased with an increase in the fiber content. Lukiantchuki *et al.* (2021) also reported that the compressive strength of fiber-reinforced cementitious materials improved with increasing fiber content. The comparison of the early and long-term compressive strength revealed that the lowest uniaxial compressive strength is noted for specimens reinforced with 12-mm-long fibers at 3 days of curing among the other fiber lengths, while after 28 days of curing, the highest uniaxial compressive strength is noted for specimens reinforced with 12-mm-long fibers. From these results, the early and long-term compressive strength of BF-reinforced CLSM is affected by the length and content of fibers.

4.4 Splitting tensile strength

The early and long-term tensile strength of BF-reinforced CLSM is evaluated from splitting tensile tests. Fig. 7 shows the stress–strain curves of the 3-day-cured BF-reinforced CLSM. Compared to unreinforced CLSM,

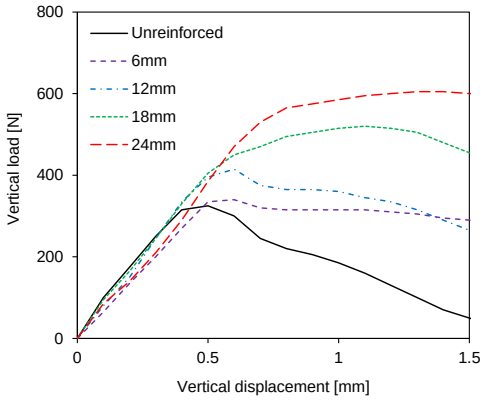

Fig. 7 Typical vertical load–displacement curves obtained from splitting tensile tests on 3 days after curing

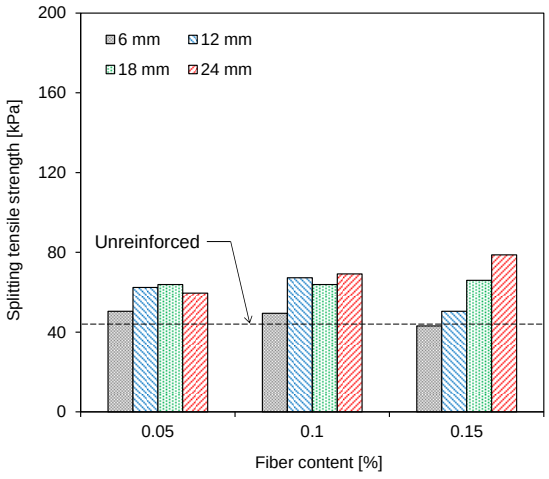

(a) 3 days

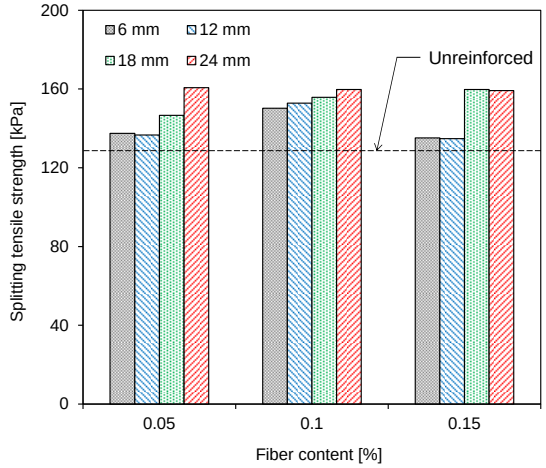

(b) 28 days

Fig. 8 Splitting tensile strength at various lengths and contents of basalt fibers

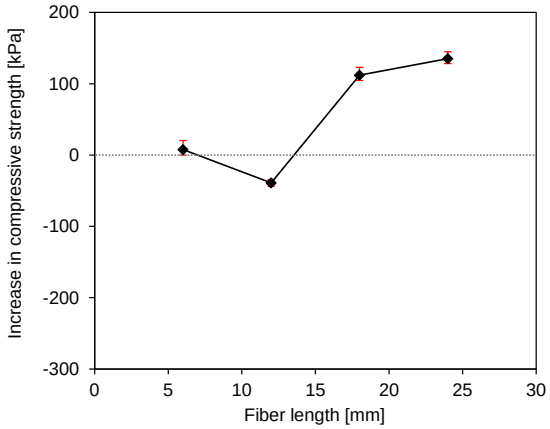

(a) 3 days

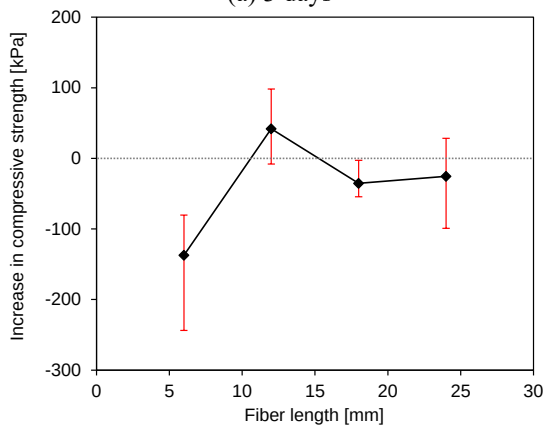

(b) 28 days

Fig. 9 Increase in uniaxial compressive strength with the fiber length

reinforced CLSM exhibits higher ductility, and ductility increase with an increase in the fiber length. The strain corresponding to the maximum splitting tensile stress also increases with an increase in the fiber length. Choi and Yuan (2005) also demonstrated that concrete incorporated with glass and PP fibers exhibited increased ductility.

Fig. 8 shows the splitting tensile strengths of CLSM as a function of the lengths and contents of BF. The red dashed line represents the splitting tensile strength of the unreinforced CLSMs, the values of which were 44 kPa and 126 kPa at curing for 3 and 28 days, respectively. Fig. 8(a) shows the splitting tensile strengths of the 3-day-cured BF-reinforced CLSM. Generally, the addition of BFs to CLSM results in an increase in the splitting tensile strength. Regardless of the fiber content, CLSMs reinforced with 6-mm-long fibers exhibit the lowest splitting tensile strength. For a fiber content of 0.15%, CLSMs reinforced with 18- and 24-mm-long fibers exhibit the two highest splitting tensile strength values. For 24-mm-long fibers, the splitting tensile strength gradually increases with an increase in the fiber content. Islam and Gupta (2016) reported that the inclusion of PP fibers in concrete up to 0.25% resulted in splitting tensile strength greater than that of the concrete without fibers, suggesting that the fibers played a role in inhibiting crack propagation within the concrete matrix. At a fiber content of 0.15%, an increase in the fiber length clearly leads to an increase in splitting tensile strength. Fig. 8(b) shows the splitting tensile strength of the 28-day-cured BF- reinforced CLSM. Generally, the addition of BF to CLSM results in splitting tensile strength greater than that of unreinforced CLSM. Overall, for each fiber content, longer fibers exhibit higher splitting tensile strengths. Nevertheless, the correlation between the increased fiber content and enhanced splitting tensile strength is not remarkably apparent. For the CLSMs reinforced with 6- and 12-mm-long fibers, the highest splitting tensile strength is observed at a fiber content of 0.1%. For the CLSMs reinforced with 18-mm-long fibers, an increase in the fiber content leads to an increase in the splitting tensile strength, while for the CLSMs reinforced with 24-mm-long fibers, the splitting tensile strength remains almost constant with an increase in the fiber content.

4.5 Strength enhancement

Fig. 9 shows the average values of the increase in the uniaxial compressive strength of reinforced CLSM compared to unreinforced CLSM as a function of fiber length. The uniaxial compressive strength of reinforced

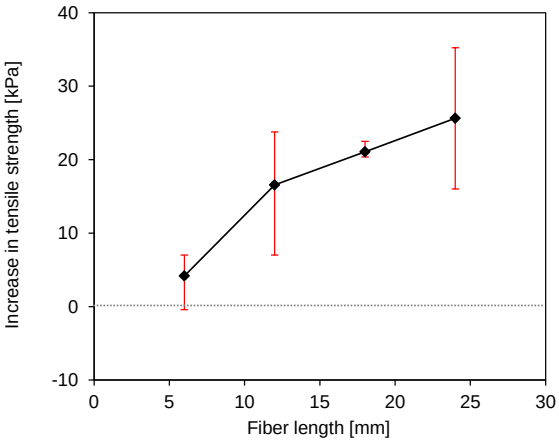

(a) 3 days

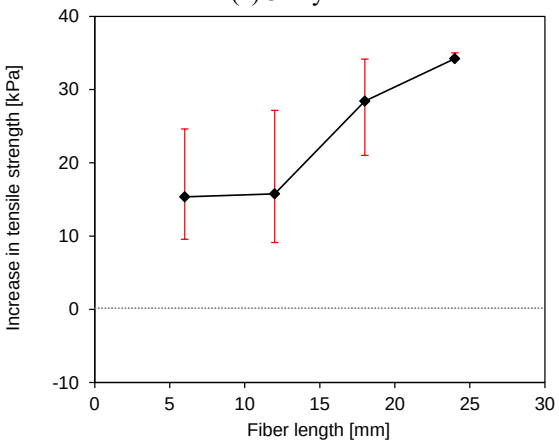

(b) 28 days

Fig. 10 Increase in splitting tensile strength with the fiber length

CLSM after 3 days of curing increases (Fig. 9(a)). As mentioned in the previous section, the change in the uniaxial compressive strength with the fiber content is almost negligible. Nevertheless, the increase in the uniaxial compressive strength depends on the fiber length. Excluding the CLSMs reinforced with 12-mm-long BF, the uniaxial compressive strength of CLSM increases with longer fiber lengths. Qian and Jiang (2023) reported that in fiber-reinforced CLSM, shorter fibers exhibited fewer contact points between them, thereby hindering the efficient distribution of stress and limiting the development of strength. In contrast, fibers of an adequate length can form a more robust network within the material. Fig. 9(b) shows changes in the increase in the uniaxial compressive strength of reinforced CLSM as a function of the fiber length after 28 days of curing. Interestingly, CLSM with a 12-mm-long fiber exhibits the highest increase in 28-day compressive strength. After 28 days of curing, the reinforced CLSMs show noticeable differences in unconfined compressive strength as the fiber content varies, compared to the results after 3 days of curing. Lu *et al.* (2022) also reported that, for basalt fiber-reinforced concrete, the variation in compressive strength at positive temperatures of curing increased with increasing basalt fiber content during long-term curing, compared to early-age curing. It is found that the increase in uniaxial compressive strength of reinforced CLSM after 28 days of curing could be influenced by the length and content of BF. Particularly, at fiber lengths greater than 12 mm, the increase in uniaxial compressive strength remains almost constant.

Fig. 10 shows the average increase in the splitting tensile strength of fiber-reinforced CLSM compared to unreinforced CLSM as a function of the fiber length. Overall, the splitting tensile strength of reinforced CLSMs increase with an increase in the fiber length regardless of the curing period. Fig. 10(a) shows the change in the splitting tensile strength of CLSMs after 3 days of curing. After 28 days of curing, the average increase in the splitting tensile strength of fiber-reinforced CLSM also increases with the fiber length (Fig. 10(b)). Furthermore, with an increase in the fiber length, the deviation in the increase of splitting tensile strength due to the fiber content decrease. Ahmad *et al.* (2020) also reported a lower splitting tensile strength of concrete mixed with shorter fibers due to insufficient bridging effects, whereas the splitting tensile strength of concrete with longer fibers was greater than that of concrete without fibers, attributed to an effective bridging effect.

4.6 Microstructure

The microstructure of BF and the bonding structure of BF-incorporated CLSM are analyzed by SEM, which was effective for investigating the morphology of hydration products in cementitious materials (Jiang *et al.* 2010). Fig. 11(a) represents the formation of ettringite resulting from the hydration reaction in the unreinforced CLSM. Ettringite, one of the most common hydration products, characterized by its needle-like or linear morphology, is formed in the SEM image, showing linear or radiating clusters. BF exhibits a multifilament structure comprising bundled monofilaments (Fig. 11(b)). Fig. 11(c) shows the network between CLSM and BF in the 28-day-cured specimen of BF-reinforced CLSM with a fiber content of 0.05%. The multifilament structure of BF is partially decomposed into monofilaments, which are embedded and bonded within the matrix. This transformation from multifilament to monofilaments is clearly identified at higher fiber contents, as shown in Figs. 11(d) and 11(e). This microstructural change can be attributed to the mixing process, which facilitates the separation and uniform incorporation of the BF monofilaments into the specimen. The results demonstrate that for a 0.05% BF content, CLSM with a fiber length of 6 mm shows lower flowability and higher setting times, compared to CLSMs with longer fiber lengths. Note that the shortest fiber length of 6 mm, among the four different lengths tested, is the most susceptible to transitioning from a multifilament structure to monofilaments. Ahmad *et al.* (2018) also analyzed the interaction of BF within mortar by SEM and found that in specimens containing more than 0.5% BF by the total weight, the fibers exhibited flocculation, which reduced the bond between the fibers and mortar. Given that the fiber content incorporated into the CLSM is less than 0.15% of the total weight, the fiber flocculation is rarely observed.

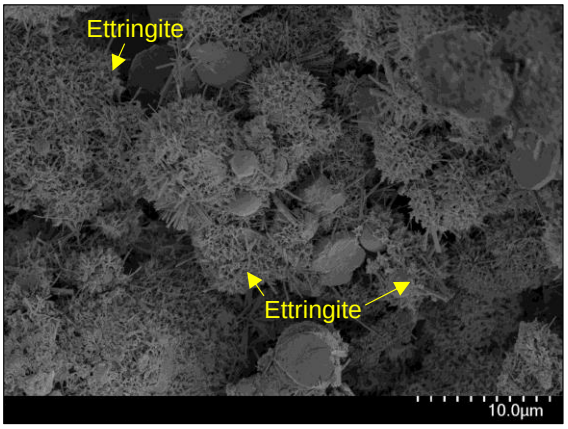

(a) Unreinforced CLSM

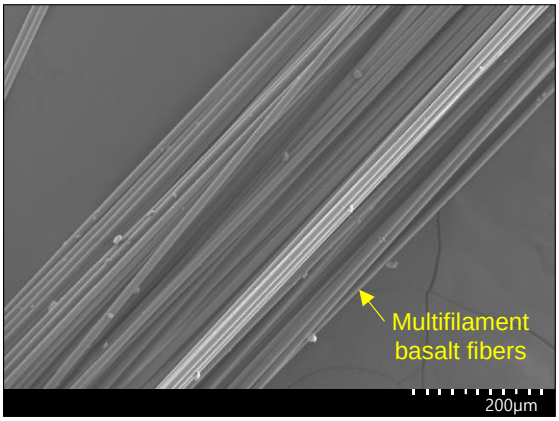

(b) BF

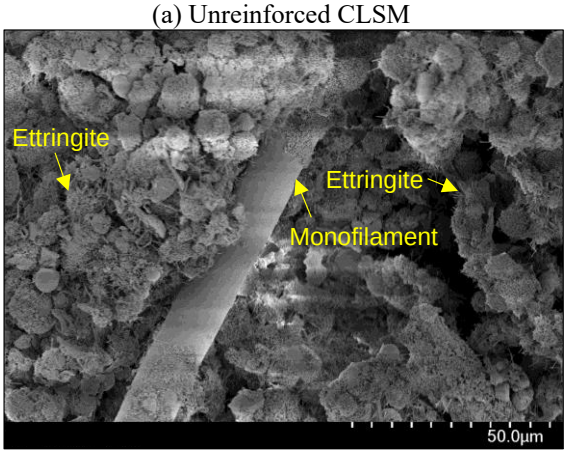

(c) Reinforced CLSM (BF content = 0.05%)

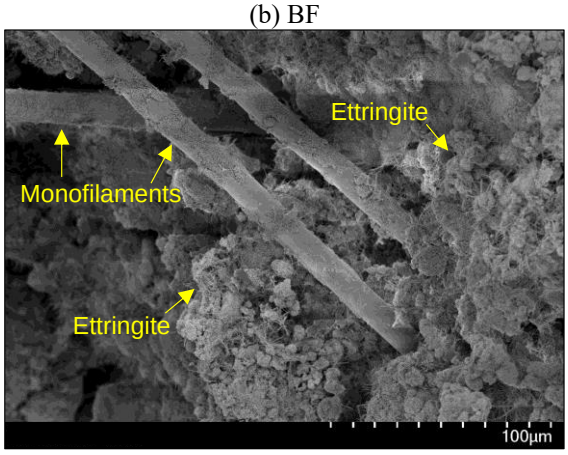

(d) Reinforced CLSM (BF content = 0.10%)

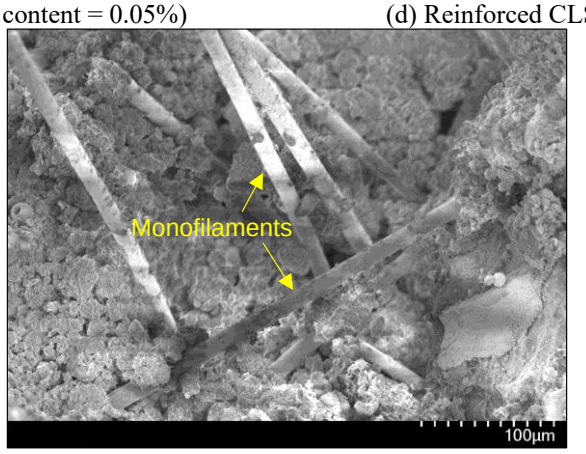

(e) Reinforced CLSM (BF content = 0.15%)

Fig. 11 Scanning electron microscopy images

5. Conclusions

In this study, the compressive and tensile strength characteristics of CLSM reinforced with BF were evaluated as a function of the fiber length and fiber content. CLSM was prepared by mixing Portland cement, fly ash, sand, and water. BF with four lengths were mixed at three fiber contents and then cured for 3 and 28 days. In addition, flowability was assessed by flow tests to determine the effect of the incorporated BF. The Vicat needle test was conducted to identify the initial and final setting times of the fiber-reinforced CLSM compared to unreinforced CLSM. The compressive and tensile strengths were evaluated by uniaxial compression tests and splitting tensile strength tests, respectively. The key findings of this study were as follows:

- The flow values of all BF-reinforced CLSM specimens decreased compared with those of the specimens without fibers. With an increase in the fiber content, flowability decreased. Notably, the most considerable reduction in flowability was observed by the addition of 6-mm-long fibers.
- Overall, the initial and final setting times of BF-reinforced specimens decreased compared with those of the specimens without fibers. Generally, with an

increase in the fiber content, the initial setting times increased, while with an increase in the content of the 6-mm-long fibers, the final setting times decreased. In contrast, a consistent trend was not observed for BF-reinforced specimens with a fiber length of 12–24 mm in terms of fiber content.

- The compressive strength of BF-reinforced specimens with fiber lengths of 18 and 24 mm after 3 days of curing was greater than that of unreinforced specimens. After 28 days, the advantages of fiber reinforcement were subtle, with some reinforced specimens even exhibiting compressive strength less than that of the unreinforced specimens.
- In terms of tensile strength, the addition of BF to CLSM generally enhanced its ductility as well as the corresponding strain at the maximum stress, particularly with longer fibers. This enhancement was consistent across a range of fiber lengths and contents. After 28 days of curing, the trend of the tensile strength increases with longer fiber lengths continued, although the relationship between the fiber content and tensile strength was not clear.
- The average increase in the uniaxial compressive strength and splitting tensile strength of fiber-reinforced CLSM, compared to unreinforced CLSM, generally increased with the fiber length regardless of the curing period. However, for compressive strength, the specimens reinforced with 12-mm-long fibers exhibited the lowest strength at early curing but exhibited the highest strength after 28 days of curing. The splitting tensile strength also increased with an increase in the fiber length, and the variability due to the fiber content diminished with longer fibers after 28 days of curing.
- BF exhibited a multifilament structure, comprising several monofilaments combined together. During the mixing process of reinforced CLSM, the multifilament structure of BF disintegrated into monofilaments, which then bonded with the CLSM material.

The study revealed that the extent of strength enhancement depended on the length and content of fibers added. Even a small amount of BF can effectively increase the early compressive strength and tensile strength over the short and long term.

Acknowledgments

This work was supported by the National Research Foundation of Korea (NRF) grant funded by the Korean government (MSIT) (No. RS-2021-NR060085; No. RS-2024-00456888).

References

ACI 229R-99 (2005), Report on Controlled Low-Strength Materials. ACI Committee 229, American Concrete Institute (ACI), Farmington Hills, MI.

Ahmad, M.R. and Chen, B. (2018), "Effect of silica fume and basalt fiber on the mechanical properties and microstructure of magnesium phosphate cement (MPC) mortar", *Constr. Build. Mater*, **190**, 466-478. https://doi.org/10.1016/j.conbuildmat.2018.09.143.

Ahmad, M.R., Chen, B. and Yu, J. (2019), "A comprehensive study of basalt fiber reinforced magnesium phosphate cement incorporating ultrafine fly ash", *Compos. Part B-Eng.*, **168**, 204-217. https://doi.org/10.1016/j.compositesb.2018.12.065.

Ahmad, W., Farooq, S.H., Usman, M., Khan, M., Ahmad, A., Aslam, F., Yousef, R.A. and Abduljabbar, H.A. (2020), "Effect of coconut fiber length and content on properties of high strength concrete", *Materials*, **13**(5), 1075. https://doi.org/10.3390/ma13051075.

Algin, Z. and Ozen, M. (2018), "The properties of chopped basalt fibre reinforced self-compacting concrete", *Constr. Build. Mater.*, **186**, 678-685. https://doi.org/10.1016/j.conbuildmat.2018.07.089.

ASTM International (2013), C191 Standard Test Methods for Time of Setting of Hydraulic Cement by Vicat Needle; ASTM International: West Conshohocken, PA, USA.

ASTM International. C496 Standard Test Method for Splitting Tensile Strength of Cylindrical Concrete Specimens; ASTM International: West Conshohocken, PA, USA, 2004.

ASTM International (2015), C618 Standard Specification for Coal Fly Ash and Raw or Calcined Natural Pozzolan for Use in Concrete; ASTM International: West Conshohocken, PA, USA.

ASTM International (2002), D4832 Standard Test Method for Preparation and Testing of Controlled Low Strength Material (CLSM) Test Cylinders; ASTM International: West Conshohocken, PA, USA.

ASTM International (1997), D6103 Standard Test Method for Flow Consistency of Controlled Low Strength Material (CLSM); ASTM International: West Conshohocken, PA, USA.

Bendjillali, K., Boulekbache, B. and Chemrouk, M. (2020), "Durability assessments of limestone mortars containing polypropylene fibres waste", *Adv. Concrete Constr.*, **10**(2), 171-183. \https://doi.org/10.12989/acc.2020.10.2.171.

Byun, Y.H., Han, W.J., Tutumluer, E. and Lee, J.S. (2016), "Elastic wave characterization of controlled low-strength material using embedded piezoelectric transducers", *Constr. Build. Mater.*, **127**, 210-219. https://doi.org/10.1016/j.conbuildmat.2016.09.113.

Cakir, F. (2021), "Evaluation of mechanical properties of chopped glass/basalt fibers reinforced polymer mortars", *Case Stud. Constr. Mater,* **15**, e00612. https://doi.org/10.1016/j.cscm.2021.e00612.

Choi, H. and Choi, Y.C. (2021), "Setting characteristics of natural cellulose fiber reinforced cement composite", *Constr. Build. Mater.*, **271**, 121910. https://doi.org/10.1016/j.conbuildmat.2020.121910.

Choi, Y. and Yuan, R.L. (2005), "Experimental relationship between splitting tensile strength and compressive strength of GFRC and PFRC", *Cement Concrete Res*, **35**(8), 1587-1591. https://doi.org/10.1016/j.cemconres.2004.09.010.

Dadmand, B., Pourbaba, M., Sadaghian, H. and Mirmiran, A. (2020), "Effectiveness of steel fibers in ultra-high-performance fiber-reinforced concrete construction", *Adv. Concrete Constr.*, **10**(3), 195-209. https://doi.org/10.12989/acc.2020.10.3.195.

Deák, T. and Czigány, T. (2009), "Chemical composition and mechanical properties of basalt and glass fibers: a comparison", *Text. Res. J.*, **79**(7), 645-651. https://doi.org/10.1177/0040517508095597.

Do, T.M. and Kim, Y.S. (2016), "Engineering properties of controlled low strength material (CLSM) incorporating red mud", *Int. J. Geo-Eng.*, **7**, 1-17. https://doi.org/10.1186/s40703-016-0022-y.

Fediuk, R., Makarova, N., Qader, D.N., Kozin, A., Amran, M., Petropavlovskaya, V. and Novichenkova, T. (2023), "Combined

effect on properties and durability performance of nanomodified basalt fiber blended with bottom ash-based cement concrete: ANOVA evaluation", *J. Mater. Res. Technol-JMRT*, **23**, 2642-2657. https://doi.org/10.1016/j.jmrt.2023.01.179.

Ge, L., Zhang, Y., Sayed, U. and Li, H. (2023), "Study on properties of basalt fiber reinforcing reactive powder concrete under different curing conditions", *J. Mater. Res. Technol-JMRT*, **27**, 5739-5751. https://doi.org/10.1016/j.jmrt.2023.10.289.

Ghanad, D.A. and Soliman, A.M. (2021), "Bio-based alkali-activated controlled low strength material: Engineering properties", *Constr. Build. Mater*, **279**, 122445. https://doi.org/10.1016/j.conbuildmat.2021.122445.

Gomaa, A.E., Hasan, A.M., Mater, Y.M. and AbdelSalam, S.S. (2023), "Shell folded footings using different angles and EPS cavity filling: experimental study", *Int. J. Geo-Eng.*, **14**(1), 10. https://doi.org/10.1186/s40703-023-00187-w.

Han, W.J, Lee, J.S., Jeong, S.H., Lim, D.S. and Byun, Y.H. (2021b), "Evaluation of engineering properties of expandable foam grout with admixture content", *Constr. Build. Mater*, **293**, 123488. https://doi.org/10.1016/j.conbuildmat.2021.123488.

Han, W.J, Lee, J.S., Kang, S., Yun, T.S. and Byun, Y.H. (2023), "Permanent deformation characteristics of expandable foam grout under cyclic loading", *Constr. Build. Mater.*, **398**, 132458. https://doi.org/10.1016/j.conbuildmat.2023.132458.

Han, W.J., Kim, S.Y., Lee, J.S. and Byun, Y.H. (2019), "Friction behavior of controlled low strength material–soil interface", *Geomech. Eng.*, **18**(4), 407-415. https://doi.org/10.12989/gae.2019.18.4.407.

Han, W.J., Lee, J.S., and Byun, Y.H. (2021a), "Volume, strength, and stiffness characteristics of expandable foam grout", *Constr. Build. Mater.*, **274**, 122013. https://doi.org/10.1016/j.conbuildmat.2020.122013.

Heo, Y.G., Son, D.G., Babatunde, Q.O. and Byun, Y.H. (2024), "Controlled low strength material modified with lignosulfonate", *Int. J. Geo-Eng.*, **15**(1), 25. https://doi.org/10.1186/s40703-024-00229-x.

Islam, G.S. and Gupta, S.D. (2016), "Evaluating plastic shrinkage and permeability of polypropylene fiber reinforced concrete", *Int. J. Sustain. Built. Environ.*, **5**(2), 345-354. https://doi.org/10.1016/j.ijsbe.2016.05.007.

Jamshaid, H. and Mishra, R. (2016), "A green material from rock: basalt fiber–a review", *J. Textile Institute*, **107**(7), 923-937. https://doi.org/10.1080/00405000.2015.1071940.

Jiang, C., Fan, K., Wu, F. and Chen, D. (2014), "Experimental study on the mechanical properties and microstructure of chopped basalt fibre reinforced concrete", *Mater. Des.*, **58**, 187-193. https://doi.org/10.1016/j.matdes.2014.01.056.

Jiang, C.H., McCarthy, T.J., Chen, D. and Dong, Q.Q. (2010), "Influence of basalt fiber on performance of cement mortar", *Key. Eng. Mater.*, **426**, 93-96. https://doi.org/10.4028/www.scientific.net/KEM.426-427.93.

Kalantari, B. and Rezazade, R.K. (2015), "Compressibility behaviour of peat reinforced with precast stabilized peat columns and FEM analysis", *Geomech. Eng.*, **9**(4), 415-426. https://doi.org/10.12989/gae.2015.9.4.415.

Kalantari, B., Prasad, A. and Huat, B.B. (2010), "Peat stabilization using cement, polypropylene and steel fibres", *Geomech. Eng.*, **2**(4), 321-335. https://doi.org/10.12989/gae.2010.2.4.321.

Khadka, S.D., Okuyucu, O., Jayawickrama, P.W. and Senadheera, S. (2023), "Controlled low strength materials (CLSM) activated with alkaline solution: Flowability, setting time and microstructural characteristics", *Case Stud. Constr. Mater.*, **18**, e01892. https://doi.org/10.1016/j.cscm.2023.e01892.

Kim, D.J., Son, D.G., Lee, J.S., Kang, T.H.K., Yun, T.S. and Byun, Y.H. (2023), "Characterization of stacked geotextile tube structure using digital image correlation", *Comput. Concrete* **31**(5), 385-394. https://doi.org/10.12989/cac.2023.31.5.385.

Kim, S.C., Kim, D.J. and Byun, Y.H. 2021. (2021), "Effect of fly ash on strength and stiffness characteristics of controlled low-strength material in shear wave monitoring", *Materials*, **14**(11), 3022. https://doi.org/10.3390/ma14113022.

Lam, T.F. and Yatim, J.M. (2015), "Mechanical properties of kenaf fiber reinforced concrete with different fiber content and fiber length", *J. Asian Concrete Federation*, **1**(1), 11-21. https://doi.org/10.18702/acf.2015.09.1.11.

Lee, J.C. and Lee, C.J. (2022), "Electro-mechanical impedance technique for assessing the setting time of steel-fiber-reinforced mortar using embedded piezoelectric sensor", *Appl. Sci.-Basel*, **12**(8), 3964. https://doi.org/10.3390/app12083964.

Lee, J.S., Han, W.J., Kim, S.Y. and Byun, Y.H. (2020), "Shear strength and interface friction characteristics of expandable foam grout", *Constr. Build. Mater.*, **249**, 118719. https://doi.org/10.1016/j.conbuildmat.2020.118719.

Lee, N.K., Kim, H.K., Park, I.S. and Lee, H.K. (2013), "Alkali-activated, cementless, controlled low-strength materials (CLSM) utilizing industrial by-products", *Constr. Build. Mater*, **49**, 738-746. https://doi.org/10.1016/j.conbuildmat.2013.09.002.

Li, Z., Shen, A., Chen, Z., Guo, Y. and Yang, X. (2022), "Research progress on properties of basalt fiber-reinforced cement concrete", *Mater. Today Commun.*, 104824. https://doi.org/10.1016/j.mtcomm.2022.104824.

Lu, J., Liu, J., Yang, H., Gao, J., Wan, X. and Zhang, J. (2022), "Influence of curing temperatures on the performances of fiber-reinforced concrete", *Constr. Build. Mater.*, **339**, 127640. https://doi.org/10.1016/j.conbuildmat.2022.127640.

Lukiantchuki, J.A., de Oliveira, J.R.M.D.S., de Almeida, M.D.S. S., dos Reis, J.H.C., Silva, T.B. and Guideli, L.C. (2021), "Geotechnical behavior of Construction Waste (CW) as a partial replacement of a lateritic soil in fiber-reinforced cement mixtures", *Geotech. Geol. Eng.*, **39**, 919-942. https://doi.org/10.1007/s10706-020-01533-w.

Ma, J., Qiu, X., Cheng, L. and Wang, Y. (2011), "Experimental research on the fundamental mechanical properties of presoaked basalt fiber concrete", *InAdvances in FRP Composites in Civil Engineering: Proceedings of the 5th International Conference on FRP Composites in Civil Engineering (CICE 2010)*, Sep 27-29, 2010, Beijing, China.

Morova, N. (2013), "Investigation of usability of basalt fibers in hot mix asphalt concrete", *Constr. Build. Mater.*, **47**, 175-180. https://doi.org/10.1016/j.conbuildmat.2013.04.048.

Okuyucu, O., Jayawickrama, P. and Senadheera, S. (2019), "Mechanical properties of steel fiber–reinforced self-consolidating controlled low-strength material for pavement base layers", *J. Mater. Civ. Eng.*, **31**(9), 04019177. https://doi.org/10.1061/(ASCE)MT.1943-5533.0002816.

Park, S.M., Lee, N.K. and Lee, H.K. (2017), "Circulating fluidized bed combustion ash as controlled low-strength material (CLSM) by alkaline activation", *Constr. Build. Mater.*, **156**, 728-738. https://doi.org/10.1016/j.conbuildmat.2017.09.001.

Punurai, W., Kroehong, W., Saptamongkol, A. and Chindaprasirt, P. (2018), "Mechanical properties, microstructure and drying shrinkage of hybrid fly ash-basalt fiber geopolymer paste", *Constr. Build. Mater.*, **186**, 62-70. https://doi.org/10.1016/j.conbuildmat.2018.07.115.

Qian, Y. and Jiang, M. (2023), "The influence of fiber on the mechanical properties of controllable low-strength materials", *Materials*, **16**(15), 5287. https://doi.org/10.3390/ma16155287.

Safdar, M., Newson, T. and Shah, F. (2021), "Consolidated drained (CID) behavior of fibre reinforced cemented Toyoura sand in triaxial loading conditions", *Int. J. Geo-Eng.*, **12**(1), 27. https://doi.org/10.1186/s40703-021-00165-0.

Shelote, K.M., Gavali, H.R., Bras, A. and Ralegaonkar, R.V. (2021), "Utilization of co-fired blended ash and chopped basalt

fiber in the development of sustainable mortar", *Sustainability*, **13**(3), 1247. https://doi.org/10.3390/su13031247.

Xiao, R., Polaczyk, P., Jiang, X., Zhang, M., Wang, Y. and Huang, B. (2021), "Cementless controlled low-strength material (CLSM) based on waste glass powder and hydrated lime: Synthesis, characterization and thermodynamic simulation", *Constr. Build. Mater.*, **275**, 122157. https://doi.org/10.1016/j.conbuildmat.2020.122157.

Xu, J., Kang, A., Wu, Z., Xiao, P. and Gong, Y. (2021), "Effect of high-calcium basalt fiber on the workability, mechanical properties and microstructure of slag-fly ash geopolymer grouting material", *Constr. Build. Mater.*, **302**, 124089. https://doi.org/10.1016/j.conbuildmat.2021.124089.

Zadehmohamad, M., Bazaz, J.B., Riahipour, R. and Farhangi, V. (2021), "Physical modeling of the long-term behavior of integral abutment bridge backfill reinforced with tire-rubber", *Int. J. Geo-Eng.*, **12**, 1-19. https://doi.org/10.1186/s40703-021-00163-2.

IC